Highlights

>The constitutive model for rate-dependent deformation of nanotwinned metals are developed.

>The athermal and thermal flow behaviors are accounted for in the model.

>The model shows good agreement with experimental results of nanotwinned coppers.

>The stress-strain relations for various strain rate and temperatures are forecasted.

TITLE

Modeling the strain rate-dependent constitutive behavior in nanotwinned polycrystalline metals

Zizheng Guo[1], Kai Wu[1], Haihui Ruan[2*], Linli Zhu[1*]

[1]Department of Engineering Mechanics, and Key Laboratory of Soft Machines and Smart Devices of Zhejiang Province, Zhejiang University, Hangzhou 310027, China

[2]Department of Mechanical Engineering, The Hong Kong Polytechnic University, Hong Kong, China

[*] Authors to whom correspondence should be addressed; electronic mail: llzhu@zju.edu.cn (Linli Zhu) and haihui.ruan@polyu.edu.hk (Haihui Ruan).

Abstract

Experimental studies have demonstrated that both strain rate and temperature influence the mechanical behavior of nanostructured metals significantly. In this work, a theoretical model is developed to describe the strain-rate-dependent constitutive behavior of nanotwinned polycrystalline metals. The athermal flow stress and thermal-activated flow stress are both considered in modeling the plastic deformation of a nanotwinned metal. Numerical results are consistent with the experimental results, showing that the present model can well describe the strain rate-dependent deformation behavior of nanotwinned polycrystalline copper. Henceforth, the constitutive behaviors of nanotwinned copper at different strain rates and temperatures can be predicted, which will be useful for optimizing the dynamic mechanical properties at various temperatures for nanotwinned metals.

Keywords: Nanotwinned metals; Strain rate; Constitutive model; Twin spacing.

1. Introduction

The development of modern industry has led to an increasing demand for both high strength and good ductility of metallic materials [1,2], while the traditional strengthening methods, such as severe plastic deformation, solid-solution, phase change, and grain refinement, are associated with the decrease in plasticity and work hardening rate [3-6]. Therefore, how to balance strength and ductility has become an important issue and the frontier in metallic materials research [7-11]. With the maturity of material preparation technology and the development of nanotechnology, people can effectively regulate the microstructural composition and size in metallic materials, making it possible to obtain high strength and high ductility in materials. Over the past two decades, researchers have developed novel nanostructured metallic materials, including nanotwinned metals [12,13], bimodal/multimodal nanostructured metals [14,15], gradient nanostructured metals [16-19] and amorphous-nanocrystalline dual phase metals [10,11]. Engineering the nanoscale twin lamellae is an effective way to achieve high-strength and high-ductility metallic materials. Experimental studies have shown that it is not complicated to form nanotwinned structures in metals. For example, one can prepare nanotwinned metallic metals through plastic deformation, phase change, annealing and other physical and chemical processes [20-23]. Currently, researchers have done a lot of experimental work on mechanical properties of nanotwinned metallic materials [12, 13, 20-22]. For example, Lu and his collaborators constructed nanoscale twin lamellae in polycrytalline copper, copper-zinc alloy as well as stainless steel, and found that these

nanotwinned metals exhibited excellent mechanical properties such as high yield strength, high plasticity and high work hardening rate [12, 24-26].

Most of recent studies are to explore the static mechanical properties of nanostructured metallic materials at room temperature. Due to the significance of high-strength and high-ductility metals in engineering applications and the increase of anti-impact requirements, more attention needs to be paid to the mechanical behavior of nanostructure metals under dynamic conditions [27-34]. It is well known that mechanical properties of metallic materials depend not only on the microstructures but also on the strain rate and temperature. Therefore, it is necessary to investigate the strain rate and temperature dependence of nanostructured metallic materials. The dynamic behaviors of traditional metallic materials have been studied extensively [35-41]. For example, Nemat-Nasser and Li [36] developed a physical model for rate and temperature-dependent flow stress of the face-centered cubic (fcc) and body-center cubic (bcc) metals based on the dislocation kinematics, which agreed with their experimental results. Gao [39] *et al.* found that the yield strength increases with the strain rate in oxygen-free high conductivity (OFHC) copper, and the increase of temperature reduces the yield strength while enhances the work hardening capacity. Liang [40] *et al.* studied the deformation behavior of TWIP steel under various strain rates through Synchrotron X-ray diffraction, and established a constitutive model to explain how the work hardening rate varies with strain rate. There are many phenomenological models [42,43], and physics-based constitutive models [44-46] to predict the mechanical behavior of metals at different temperatures and strain rates.

However, few of them can describe the dynamic plastic behavior of nanotwinned metals.

In this work, a constitutive model of nanotwinned metals is established on the basis of elastoplastic theory, which involves both athermal and thermal-related flow behaviors. The stress-strain response of nanotwinned metals at different strain rates and temperatures are described, and a good agreement between numerical and experimental results is obtained.

2. Theoretical model

On the basis of the relationship between deformation and the crystallography in metallic material, a material enters the plastic deformation stage when the shear stress on a slip line is greater than a critical value. Dislocations activities leads to the plastic deformation, of which the quantitative relation is the basis of a dislocation-based plasticity models. In general, linear elasticity is still assumed in the constitutive theory of metallic materials. In order to simulate the elastoplastic behavior of a nanotwinned metal, the total strain rate is decomposed into elastic strain rate and plastic strain rate, given as

$$\dot{\boldsymbol{\varepsilon}} = \dot{\boldsymbol{\varepsilon}}^{\mathrm{e}} + \dot{\boldsymbol{\varepsilon}}^{\mathrm{p}}, \tag{1}$$

where the elastic strain and stress follows the linear elasticity theory, namely,

$$\dot{\boldsymbol{\varepsilon}}^{\mathrm{e}} = \mathbf{M} : \dot{\boldsymbol{\sigma}}. \tag{2}$$

Here, M is the elastic compliance tensor. According to the traditional J_2-flow rule, the plastic strain can be expressed as

$$\dot{\boldsymbol{\varepsilon}}^{\mathrm{p}} = \frac{3\dot{\varepsilon}^{p}}{2\sigma_{e}}\boldsymbol{\sigma}', \tag{3}$$

where $\sigma_e = \sqrt{3\sigma'_{ij}\sigma'_{ij}/2}$ is the von Mises equivalent stress, $\sigma'_{ij}=\sigma_{ij}-\sigma_{kk}\delta_{ij}/3$ are deviatoric stresses. The equivalent plastic strain rate is expressed as

$$\dot{\varepsilon}^p = \dot{\varepsilon}\left[\frac{\sigma_e}{\sigma_{flow}}\right]^{m_0}, \tag{4}$$

where $\dot{\varepsilon} = \sqrt{2\dot{\varepsilon}'_{ij}\dot{\varepsilon}'_{ij}/3}$ is equivalent strain, $\dot{\varepsilon}'_{ij}=\dot{\varepsilon}_{ij}-\dot{\varepsilon}_{kk}\delta_{ij}/3$ are deviatoric strain rates, $\mathbf{m}_0$ is the rate-related parameter, σ_{flow} represents the flow stress of the nanotwinned metals. With equations (1–4), a theoretical framework to describe the stress-strain relation of the material has been obtained. **In the case of uniaxial tension of a isotropic solid, the von Mises equivalent stress equals to tensile stress, $\sigma_e = \sigma$; ε_{11} denotes the strain along the tensile direction.** Then, the components of the strain rate tensor can be derived from Eq. (1), given as

$$\begin{cases} \dot{\varepsilon}_{11} + 2\dot{\varepsilon}_{22} = \dfrac{\dot{\sigma}}{3\mathbf{K}} \\ \dfrac{2}{3}\left(\dot{\varepsilon}_{11} - \dot{\varepsilon}_{22}\right) = \dfrac{\dot{\sigma}}{3\mu} + \dot{\varepsilon}^{\mathbf{p}} \end{cases}. \tag{5}$$

Herein, $\mathbf{K}$ and μ are the bulk and shear moduli, respectively. From Eq. (4), the plastic strain rate is expressed as:

$$\dot{\varepsilon}^{\mathbf{p}} = \frac{2}{3}(\dot{\varepsilon}_{11}-\dot{\varepsilon}_{22})\left[\frac{\sigma}{\sigma_{flow}}\right]^{m_0}. \tag{6}$$

Eqs. (5) and (6) can then be used to calculate the stress-strain relation of a tensile test by solving the ordinary differentiate equations (OEDs) numerically. In the elastoplastic constitutive model introduced above, the most important issue is to have a precise description of the flow stress σ_{flow} for a nanotwinned metal.

In general, the flow stress of a material can be decomposed into an athermal part (σ_{ath}) and a thermal part (σ_{th}), given as

$$\sigma_{\text{flow}} = \sigma_{\text{ath}} + \sigma_{\text{th}}. \tag{7}$$

For a nanotwinned metal, athermal flow stress can be expressed based on the Taylor model as [48,49],

$$\sigma_{\text{ath}} = \sigma_0 + M\alpha\mu b\sqrt{\rho_{\text{TB}} + \rho_{\text{GB}} + \rho_{\text{I}}} + \sigma_{\text{b}}. \tag{8}$$

Here, σ_0 is friction stress for lattices, M, α, μ, b represent the Taylor factor, Taylor constant, shear modulus and magnitude of the Burgers vector, respectively. ρ_{TB} represents the density of dislocations piled up near the twin boundaries, and ρ_{GB} represents the density of dislocations piled up near the grain boundaries, and ρ_{I} represents the dislocation density in the crystal interior, and σ_{b} the back stress. **The exact expression of these densities of dislocations and back stress can be found in the Appendix.** The thermal part of the flow stress can be written as **[39,46]**

$$\sigma_{\text{th}} = f(\dot{\varepsilon}, T)\sigma_{\text{th}}^{*}, \tag{9}$$

where $f(\dot{\varepsilon}, T)$ and σ_{th}^{*} are both the functions of strain rate and temperature, given as

$$f(\dot{\varepsilon}, T) = \{1-[-c_2 T \ln(\frac{\dot{\varepsilon}}{\dot{\varepsilon}_0})]^{1/q}\}^{1/p}, \tag{10}$$

$$\sigma_{\text{th}}^{*} = Y\varepsilon^{n}\exp[c_3 T\ln(\frac{\dot{\varepsilon}}{\dot{\varepsilon}_{\text{s0}}})]. \tag{11}$$

Therefore, the total flow stress of the nanotwinned metals can be written as

$$\sigma_{\text{flow}} = M\mu\alpha b\sqrt{\rho_{\text{TB}} + \rho_{\text{GB}} + \rho_{\text{I}}} + Y\varepsilon^{n}\exp[c_3 T\ln(\frac{\dot{\varepsilon}}{\dot{\varepsilon}_{\text{s0}}})]\{1-[-c_2 T\ln(\frac{\dot{\varepsilon}}{\dot{\varepsilon}_0})]^{1/q}\}^{1/p}, \tag{12}$$

where Y is the reference thermal stress that is sensitive to the microstructure evolution, n and c_2 are the material constants, c_3 is related to free energy, p and q are a pair of parameters characterizing the shape of activation barrier.

3. The results and the theoretical model of discussion

The proposed elastoplastic model of nanotwinned metals is applied to simulate the constitutive behaviors with different strain rates and temperature. The experimental results of rate-dependent stress-strain relations of polycrystalline nanotwinned coppers [7] are used here for comparisons. These polycrystalline nanotwinned copper samples have the average grain size of 400 nm~500 nm with the twin spacings of 15 nm, 35 nm, and 100 nm [7]. The parameters used in calculations are taken from the existing literature [46-49], wherein the grain-size-dependent and the dynamic constitutive models are presented to calculate the mechanical properties of nanotwinned copper and dynamical mechanical behaviors of polycrystalline copper, respectively. The parameters for determining the thermal flow stress have been identified for OFHC copper in Ref. [39]. In the present work, the multi-variable nonlinear regression method is applied to determine the optimum group of those parameters for determining the thermal-part of the flow stress. The list of these parameters and their values can be found in the Table 1.

Firstly, the stress-strain relations of nanotwinned polycrystalline copper at different strain rates are calculated and compare with the experimental results. Figure 1 shows the simulated stress-strain curves of the nanotwinned copper with three different twin spacings (15nm, 30nm, 100nm) under strain rates from $6\times10^{-4}s^{-1}$ to $6\times10^{-1}s^{-1}$, wherein the experimental data are also plotted. It is found that the

numerical results well agree with the experimental results, indicating that our model can describe the stress-strain response of nanotwinned polycrystalline copper at different strain rates. **In the elastic deformation region, the calculated results deviates from those of experiments, because the elastic modulus of nanotwinned copper is greater than that of bulk polycrystalline copper without nanotwins, which has also been found in [48]. The possible cause of such a difference could be anisotropy because the nanotwinned copper samples are electro-deposited thin films with probably a narrow distribution of grain orientation. Since we only focus on the plastic deformation of polycrystalline nanotwinned coppers in this work, the difference in the elastic regime is not accounted for.**

The proposed model can also be applied to predict the relationship between flow stress and strain rate under a given strain, as shown in Figure 2. Fig. 2(a) shows the simulated flow stresses at the strains of 5% and 10% for the twin lamellae thickness of 15 nm when the strain rate is increased from $6\times10^{-4}s^{-1}$ to $6\times10^{-1}s^{-1}$. The comparison between the predictions and the experimental data is addressed. Figures 2 (b) and (c) plot the comparison of simulated flow stress with experimental results of the twin lamellae thickness of 35 nm at the strain of 5% and the twin lamellae thickness of 100 nm at the strain of 2%, respectively. As can be seen from the figure, the flow stress of the nanotwinned copper increases with the increase of the strain rate, and the predictions based on the proposed model are consistent with the experimental results [7]. **Figure 2(d) depicts the flow stress versus strain rate for the twin spacing of 15nm and 100 nm in a nanotwinned copper. It is noted that**

the slope of the curve for the twin spacing of 15 nm is slightly larger than that of the twin spacing of 100 nm.

Finally, we predict the effect of temperature and strain rate on the constitutive behavior of nanotwinned copper based on proposed theoretical model. Note that the strain rate changes from $6\times10^{-4}s^{-1}$ to $6\times10^{-1}s^{-1}$ in experiments. For higher strain rates, the predicted results are shown in figure 3(a). It is noted that the strain-hardening rate is obviously enhanced and the yield strength of the material only slightly increases when the strain rate increases from $6\times10^{-0}\mathbf{s}^{-1}$ to $6\times10^{3}\mathbf{s}^{-1}$. The reason is that the yield strength is dominated by athermal flow stress which is almost independent on the strain rate, while the strain hardening behavior mainly comes from the thermal-related part which is sensitive to the strain rate. **It also should be pointed out that the void nucleation and growth as well as the microstructural evolution can also contribute to the hardening behaviors at high strain rates [16, 34, 50-52]**. Figure 3(b) shows the stress-strain relationships between nanotwinned copper at different temperatures. From the figure, one can note that the yield stress and strain hardening capability of nanotwinned copper are both reduced with the increase in temperature. At higher temperature, the softening behavior will occurs during plastic deformation in nanotwinned copper. **Such a high temperature induced softening comes from the function $f(\dot{\varepsilon},T)=\sigma_{\mathbf{th}}/\sigma_{\mathbf{th}}^{*}$ which characterizes the thermal activation behavior. The relationship between the plastic strain rate and the average dislocation velocity v can be written as $\dot{\varepsilon}=m'b\rho_m v$ [53], wherein m' is the Schmidt factor, ρ_m is the density of moving dislocations, and**

$v=v_0\exp(-\Delta G/k_B T)$ is the average velocity of dislocations [54]. The free energy of thermal activation ΔG can be expressed as $\Delta G = G_0\left(1-\left(\sigma_{th}/\sigma_{th}^{*}\right)^{p}\right)^{q}$ with k_B being the Boltzmann constant. When the strain rate is a constant, the average dislocation velocity should be a constant. Therefore, with the increase in temperature, the free energy of thermal activation must also be enhanced. Since the *p* is in the range of 0~1 and *q* is in the range of 1~2, the thermal flow stress σ_{th} thus decreases, i.e., $f(\dot{\varepsilon},T)<1$, leading to the softening behavior.

4. Conclusion

In summary, the present work investigated the dynamic behavior of nanotwinned polycrystalline copper at different temperatures. The strain-rate-dependent elastoplastic constitutive model was developed to describe the influence of strain rate and temperature on the stress-strain relationship of a nanotwinned copper. The theoretical results show that our model can describe the strain-rate-dependent constitutive relation of a nanotwinned copper because an excellent agreement with the experimental results has been obtained. Furthermore, the mechanical behaviors of nanotwinned copper under high strain rates and various temperatures are predicted. The results show that the increase in strain rate improve the yield strength and the work hardening ability. The increase in temperature results in a reduced strength and work hardening rate. This work will provide a theoretical basis for optimizing the mechanical properties of nanotwinned metals under various strain rates and temperatures.

Acknowledgements

This research is supported by the National Natural Science Foundation of China (Grant nos. 11321202, 1147243, 11621062), and the Fundamental Research Funds for the Central Universities (Grant no. 2018XZZ001-05).

Reference

[1] G. Frommeyer, U. Brux, P. Neumann, Supra-ductile and high-strength manganese-TRIP/TWIP steels for high energy absorption purposes, ISI J. Int. 43 (2003) 438-446.

[2] B.C. DeCooman, K.G. Chin, J.K. Kim, High Mn TWIP steels for automotive applications, in: M. Chiaberge (Ed.), New Trends Dev. Automot. Syst. Eng. 2011, pp. 101-128.

[3] Y.T. Zhu, X.Z. Liao, Nanostructured metals: retaining ductility, Nat. Mater. 3 (2004) 351-352.

[4] M.A. Meyers, A. Mishra, D.J. Benson, Mechanical properties of nanocrystalline materials, Prog. Mater. Sci. 51 (2006) 427-556.

[5] O. Bouaziz, S. Allain, C.P. Scott, P. Cugy, D. Barbier, High manganese austenitic twinning induced plasticity steels: A review of the microstructure properties relationships, Curr. Opin. Solid State Mater. Sci. 15 (2011) 141-168.

[6] H. Kou, J. Lu, Y. Li, High Strength and High Ductility Nanostructured and Amorphous Metallic Materials, Adv. Mater. 26 (2014) 5518-5524.

[7] M. Dao, L. Lu, R.J. Asaro, J.T.M. De Hosson, E. Ma, Toward a quantitative understanding of mechanical behavior of nanocrystalline metals, Acta Mater. 55 (2007) 4041-4065.

[8] R.O. Ritchie, The conflicts between strength and toughness, Nat. Mater. 10 (2011) 817-822.

[9] K. Lu, Making strong nanomaterials ductile with gradients, Science 345 (2014) 1455-1456.

[10] J. Hu, Y.N. Shi, X. Sauvage, G. Sha, K. Lu, Grain boundary stability governs hardening and softening in extremely fine nanograined metals, Science 355 (2017) 1292-1296.

[11] G. Wu, K.C. Chan, L. Zhu, L. Sun, J. Lu, Dual-phase nanostructuring as a route to high-strength magnesium alloys, Nature 545 (2017) 80-83.

[12] L. Lu, Y.F. Shen, X.H. Chen, L.H. Qian, K. Lu, Ultrahigh strength and high electrical conductivity in Copper, Science 304 (2004) 422-426.

[13] L. Lu, X. Chen, X. Huang, K. Lu, Revealing the maximum strength in nanotwinned copper, Science 323 (2009) 607-610.

[14] Y. Wang, M. Chen, F. Zhou, E. Ma, High tensile ductility in a nanostructured metal, Nature 419 (2002) 912-915.

[15] Y. Zhao, T. Topping, J.F. Bingert, J.J. Thornton, A.M. Dangelewicz, Y. Li, W. Liu, Y. Zhu, Y.Z. Zhou, E.J. Lavernia, High Tensile Ductility and Strength in Bulk Nanostructured Nickel, Adv. Mater. 20 (2010) 3028-3033.

[16] A.Y. Chen, H.H. Ruan, J. Wang, H.L. Chan, Q. Wang, Q. Li, J. Lu, The

influence of strain rate on the microstructure transition of 304 stainless steel, Acta Mater. 59 (2011) 3697-3709.

[17] Y. Wei, Y. Li, L. Zhu, L.C. Zhu, Y. Liu, X.Q. Lei, G. Wang, Y.X. Wu, Z.L. Mi, J.B. Liu, H.T. Wang, H.J. Gao, Evading the strength-ductility trade-off dilemma in steel through gradient hierarchical nanotwins, Nat. Commun. 5 (2014) 3580.

[18] X. Tan, Y. Kok, Y.J. Tan, M. Descoins, D. Mangelinck, S.B. Tor, K.F. Leong, Graded microstructure and mechanical properties of additive manufactured Ti-6Al-4V via electron beam melting, Acta Mater. 97 (2015) 1-16.

[19] X.L. Wu, M.X. Yang, F.P. Yuan, L. Chen, Y.T. Zhu, Combining gradient structure and TRIP effect to produce austenite stainless steel with high strength and ductility, Acta Mater. 112 (2016) 337-346.

[20] K. Lu, L. Lu, S. Suresh, Strengthening materials by engineering coherent internal boundaries at the nanoscale, Science 324 (2009) 349-352

[21] P. Müllner, A.H. King, Deformation of hierarchically twinned martensite, Acta Mater. 58 (2010) 5242-5261.

[22] Z.J. Zhang, H.W. Sheng, Z.J. Wang, B. Gludovatz, Z. Zhang, E.P. George, Q. Yu, S.X. Mao, R.O. Ritchie, Dislocation mechanisms and 3D twin architectures generate exceptional strength-ductility-toughness combination in CrCoNi medium-entropy alloy, Nat. Commun. 8 (2017) 14390.

[23] L. Sun, X. He, J. Lu, Nanotwinned and hierarchical nanotwinned metals: a review of experimental, computational and theoretical efforts, NPJ Comput. Mater. 6 (2018) 1-18.

[24] G.H. Xiao, N.R. Tao, K. Lu, Microstructures and mechanical properties of a Cu-Zn alloy subjected to cryogenic dynamic plastic deformation, Mater. Sci. Eng. A. 513-514 (2009) 13-21.

[25] G.H. Xiao, N.R. Tao, K. Lu, Strength-ductility combination of nanostructured Cu-Zn alloy with nanotwin bundles, Scr. Mater. 65 (2011) 119-122.

[26] H.T. Wang, N.R. Tao, K. Lu, Strengthening an austenitic Fe-Mn steel using nanotwinned austenitic grains, Acta Mater. 60 (2012) 4027-4040.

[27] R. Kuziak, R. Kawalla, S. Waengler, Advanced high strength steels for automotive industry, Arch. Civil. Mech. Eng. 8 (2008) 103-117.

[28] O. Bouaziz, H. Zurob, M. Huang, Driving force and logic of development of advanced high strength steels for automotive applications, Steel Res. Int. 84 (2013) 937-947.

[29] H. Kim, D.W. Suh, N.J. Kim, Fe-Al-Mn-C lightweight structural alloys: a review on the microstructures and mechanical properties, Sci. Technol. Adv. Mater. 14 (2013) 014205.

[30] J. Frontán, Y. Zhang, M. Dao, J. Lu, F. Gálvez, A. Jérusalem, Acta Mater. 60 (2012) 1353-1367.

[31] A. Jérusalem, W. Dickson, M.J. Pérez-Martín, M. Dao, J. Lu, F. Gálvez, Scr. Mater. 69 (2013) 773-776.

[32] Z.Y. Liang, X. Wang, W. Huang, M.X. Huang, Acta Mater. 88 (2015) 170-179.

[33] J.T. Fan, Rate dependency of a Zr-based bulk metallic glass: Strength and fracture characteristic, Mater. Lett. 216 (2018) 176-178.

[34] J.T. Fan, M.Q. Jiang, Strain hardenability of a gradient metallic alloy under high-strain-rate compressive loading, Mater. Des. 170 (2019) 107695.

[35] P.S. Follansbee, U.F. Kocks, A constitutive description of the deformation of copper based on the use of the mechanical threshold stress as an internal state variable, Acta Metall. 36 (1988) 81-93.

[36] S. Nemat-Nasser, Y. Li, Flow stress of f.c.c. polycrystals with application to OFHC Cu, Acta Mater. 46 (1998) 565-577.

[37] W.S. Lee, C.F. Lin, Impact properties and microstructure evolution of 304L stainless steel, Mater. Sci. Eng. A. 308 (2001) 124-135.

[38] M.A. Meyers, D.J. Benson, O. Vöhringer, et al. Constitutive description of dynamic deformation: physically-based mechanisms, Mater. Sci. Eng. A. 322 (2002) 194-216.

[39] C.Y. Gao, L.C. Zhang, A constitutive model for dynamic plasticity of FCC metals, Mater. Sci. Eng. A. 527 (2010) 3138-3143.

[40] Z.Y. Liang, X. Wang, W. Huang, M.X. Huang, Strain rate sensitivity and evolution of dislocations and twins in a twinning-induced plasticity steel, Acta Mater. 88 (2015) 170-179.

[41] Y.F. Shen, N. Jia, R.D.K. Misra, L. Zuo, Softening behavior by excessive twinning and adiabatic heating at high strain rate in a Fe-20mn-0.6c twip steel, Acta Mater. 103 (2016) 229-242.

[42] J.L. Chaboche, A review of some plasticity and viscoplasticity constitutive theories, Int. J. Plast. 24 (2008) 1642-1693.

[43] Y.C. Lin, X.M. Chen, A critical review of experimental results and constitutive descriptions for metals and alloys in hot working, Mater. Des. 32 (2011) 1733-1759.

[44] G.Z. Voyiadjis, A.H. Almasri. A physically based constitutive model for fcc metals with applications to dynamic hardness, Mech. Mater. 40 (2008) 549-563.

[45] F. Roters, P. Eisenlohr, L. Hantcherli, D.D. Tjahjanto, T.R. Bieler, D. Raabe. Overview of constitutive laws, kinematics, homogenization and multiscale methods in crystal plasticity finite-element modeling: Theory, experiments, applications, Acta Mater. 58 (2010) 1152-1211.

[46] C.Y. Gao, L.C. Zhang. Constitutive modelling of plasticity of fcc metals under extremely high strain rates, Int. J. Plast. 32-33 (2012) 121-133

[47] J.W. Hutchinson, Bounds and Self-Consistent Estimates for Creep of Polycrystalline Materials, Proc. R. Soc. A Math. Phys. Eng. Sci. 348 (1976) 101-127.

[48] L.L. Zhu, H.H. Ruan, X.Y. Li, M. Dao, H.J. Gao, J. Lu, Modeling grain size dependent optimal twin spacing for achieving ultimate high strength and related high ductility in nanotwinned metals, Acta Mater. 59 (2011) 5544- 5557.

[49] L.L. Zhu, S.X. Qu, X. Guo, J. Lu, Analysis of the twin spacing and grain size effects on mechanical properties in hierarchically nanotwinned face-centered cubic metals based on a mechanism-based plasticity model, J. Mech. Phys. Solids. 76 (2015) 162-179.

[50] **J. Belak, On the nucleation and growth of voids at high strain-rates, J.**

Comput. -Aided. Mat. Des. 5 (1998) 193-206.

[51] X. Yang, X.G. Zeng, J. Wang, J.B. Wang, F. Wang, J. Ding, Atomic-scale modeling of the void nucleation, growth, and coalescence in Al at high strain rates, Mech. Mater. 135 (2019) 98-113.

[52] R. Thevamaran, O. Lawal, S. Yazdi, S. J. Jeon, J. H. Lee, E. L. Thomas, Dynamic creation and evolution of gradient nanostructure in single-crystal metallic microcubes. Science, 354 (2016) 312-316.

[53] E. Orowan, Problems of plastic gliding, Proc. Proc. Phys. Soc. 52 (1940) 8-22.

[54] W.G. Johnston, J.J. Gilman, Dislocation velocities, dislocation densities, and plastic flow in lithium fluoride crystals, J. Appl. Phys. 30 (1959) 129-144.

Appendix.

The athermal flow stress for the polycrystalline nanotwinned metals can be expressed in the Taylor model, given as [48, 49]

$$\sigma_{\text{flow}}^{\text{T}} = \sigma_0 + M\alpha\mu b\sqrt{\rho_{\text{I}} + \rho_{\text{TB}} + \rho_{\text{GB}}} + \sigma_{\text{b}}. \tag{A1}$$

Here, ρ_{TB} is the density of dislocations piled up long the twin boundaries and dependent on the grain size d_{G} and twin spacing d_{TB}, given as [49]

$$\rho_{\text{TB}} = \frac{\Phi_0}{d_{\text{G}}{}^2} + \frac{\Phi_1}{d_{\text{G}} d_{\text{TB}}} - \frac{\Phi_2}{d_{\text{TB}}^2}, \tag{A2}$$

where Φ_0, Φ_1, and Φ_2 are the size-independent constants. ρ_{GB} is the dislocation density associated with the contribution of grain boundaries, which can be given as

[48, 49]

$$\rho_{\mathrm{GB}} = k^{\mathrm{GB}} \frac{\eta^{\mathrm{GB}}}{b} . \tag{A3}$$

Here, $k^{\mathrm{GB}} = 6d_{\mathrm{GBDPZ}} / \phi^{\mathrm{GB}} d_{\mathrm{G}}$. d_{GBDPZ} is the GBDPZ thickness and ϕ^{GB} the constant. ρ_{I} denotes the dislocation density in the crystal interior and it follows the evolution law as [48]

$$\frac{\partial \rho_{\mathrm{I}}}{\partial \varepsilon^{\mathrm{p}}} = M[\frac{1}{b d_{\mathrm{G}}} + \frac{\psi \sqrt{\rho_{\mathrm{I}}}}{b} - \psi_0 \rho_{\mathrm{I}}]. \tag{A4}$$

Here, d_{G} is the grain size, ψ is a proportionality factor. $\psi_0 = k_{20}(\dot{\varepsilon}^{\mathrm{p}} / \dot{\varepsilon}_r)^{-n_0^{-1}}$, in which k_{20} and n_0 are the constants, and $\dot{\varepsilon}_r$ is a reference strain rate. The back stress σ_{b} characters the kinematic hardening behavior and follows

$$\sigma_{\mathrm{b}} = M \frac{\mu b}{d_{\mathrm{G}}} N_{\mathrm{b}} , \tag{A5}$$

where N_{b} is the dislocation number at the grain boundaries, which follows the evolution law with respect to the plastic strain as [48]

$$\frac{dN}{d\varepsilon^{p}} = \frac{\zeta}{b}(1 - \frac{N}{N_B}) . \tag{A6}$$

Here, ζ is the mean spacing between slip bands and N_B the maximum number of dislocation loops at the grain boundaries.

Table Caption

Table 1. Description, symbol, magnitude for the different parameters of the models appear.

Figure Captions

Figure 1. The stress strain relationship between nanotwinned copper under different strain rates is compared with the experimental results [16]. (a) 15nm twin lamellae, (b) 35nm twin lamellae, (c) 100nm twin lamellae.

Figure 2. The comparison between the theoretical predictions and the experiment results for the relationship between flow stress at a given strain and strain rate. For the twin spacing of 15nm, the given strains are 5% and 10% (a), and the given strain is selected as 5% for twin spacing of 35 nm (b), and as 2% for twin spacing of 100nm. **The simulated flow stress as the function of strain rate with different twin spacing (d).**

Figure 3. Theoretical prediction of the stress strain relationship between nanotwinned copper at higher strain rate (a) and at different temperatures (b).

Table 1

Description, symbol, magnitude for the different parameters of the models appear.

Parameter (Unit)	Symbol	Magnitude
Grain size (nm)	d_{G}	500
Bulk modulus (GPa)	K	137.1
Shear modulus (GPa)	μ	47.1
Poisson's ratio	ν	0.36
Magnitude of the Burgers vector (nm)	b	0.256
Taylor factor	M	1.732~ 3.06
Taylor constant	α	0.2~0.5
Thickness of GBDPZ (nm)	d_{GBDPZ}	3.6
Thickness of TBDPZ (nm)	d_{TBDPZ}	3.6
Maximum number of dislocation	N_0	9
Mean spacing between slip bands (nm)	ζ	2
Dislocation density related parameter	Φ_0	120
Dislocation density related parameter	Φ_1	2.04×10^{4}
Dislocation density related parameter	Φ_2	2.64
Dynamic recovery constant	k_{20}	18.5
Proportionality factor	ψ	0.2
Dynamic recovery constant	n	12.25
Reference strain rate (s^{-1})	$\dot{\varepsilon}_r$	1.75
Reference thermal stress(MPa)	Y	100~1000
Constant for crystal barrier shape	p	0~1
Constant for crystal barrier shape	q	1~2
Reference strain rate(s^{-1})	$\dot{\varepsilon}_0$, $\dot{\varepsilon}_{s0}$	1.5×10^{8}, 1×10^{8}
Annihilation factor at T=0,	k_0	0.9
Nominal activation energy(1/K)	c_2 , c_3	$1.\times10^{-4}$, 8.5×10^{-5}

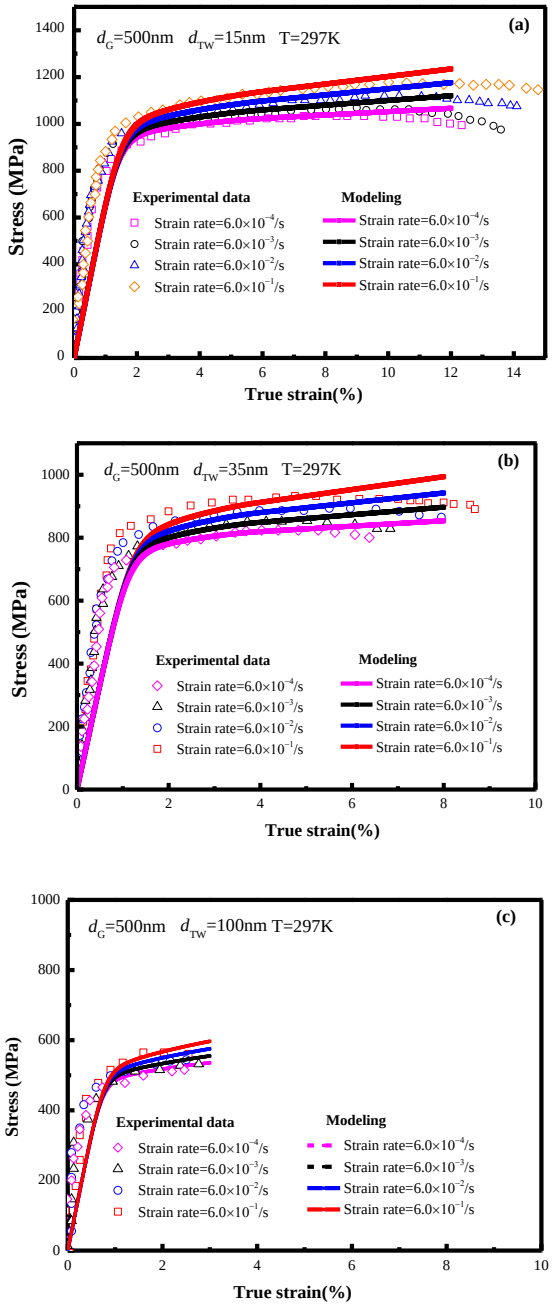

Figure 1 The stress strain relationship between nanotwinned copper under different strain rates is compared with the experimental results [16]. (a) 15nm twin lamellae, (b) 35nm twin lamellae, (c) 100nm twin lamellae.

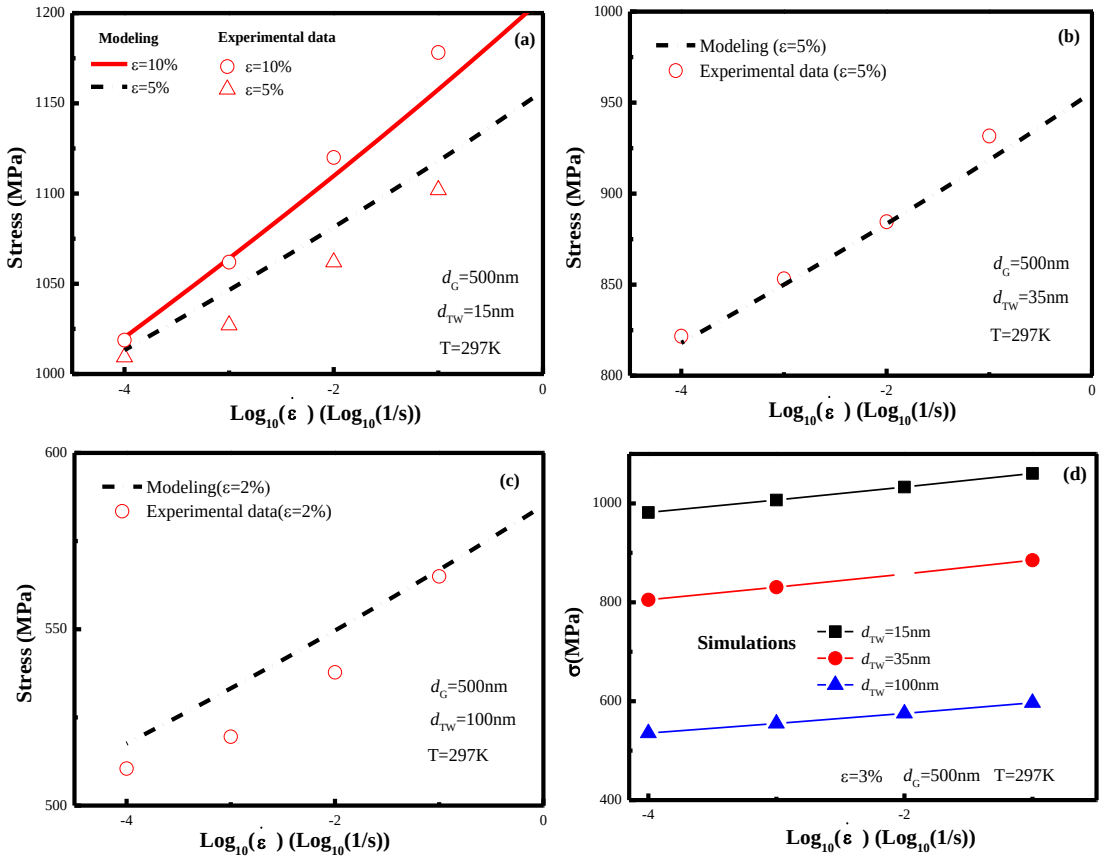

Figure 2. The comparison between the theoretical predictions and the experiment results for the relationship between flow stress at a given strain and strain rate. For the twin spacing of 15nm, the given strains are 5% and 10% (a), and the given strain is selected as 5% for twin spacing of 35 nm (b), and as 2% for twin spacing of 100nm. **The simulated flow stress as the function of strain rate with different twin spacing (d).**

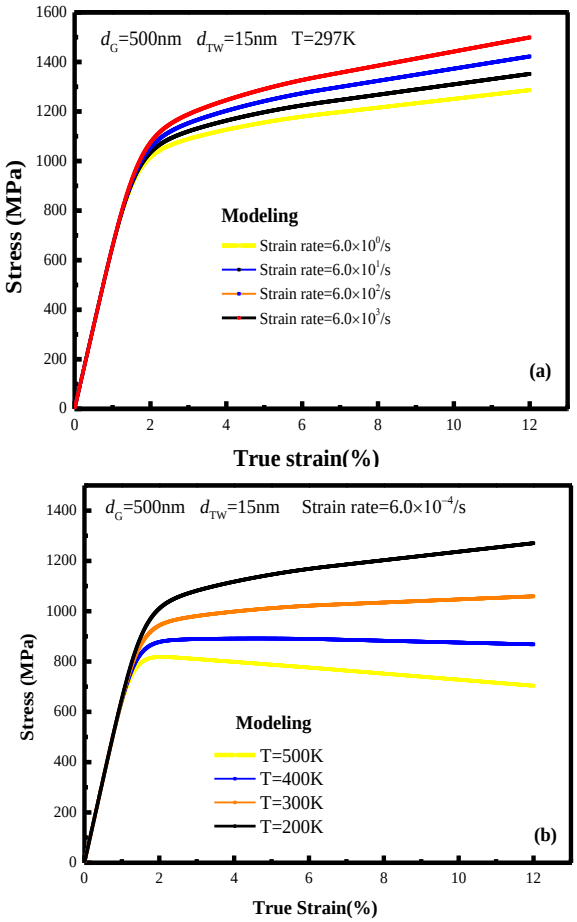

Figure 3. Theoretical prediction of the stress strain relationship between nanotwinned copper at higher strain rate (a) and at different temperatures (b).

Figure1a

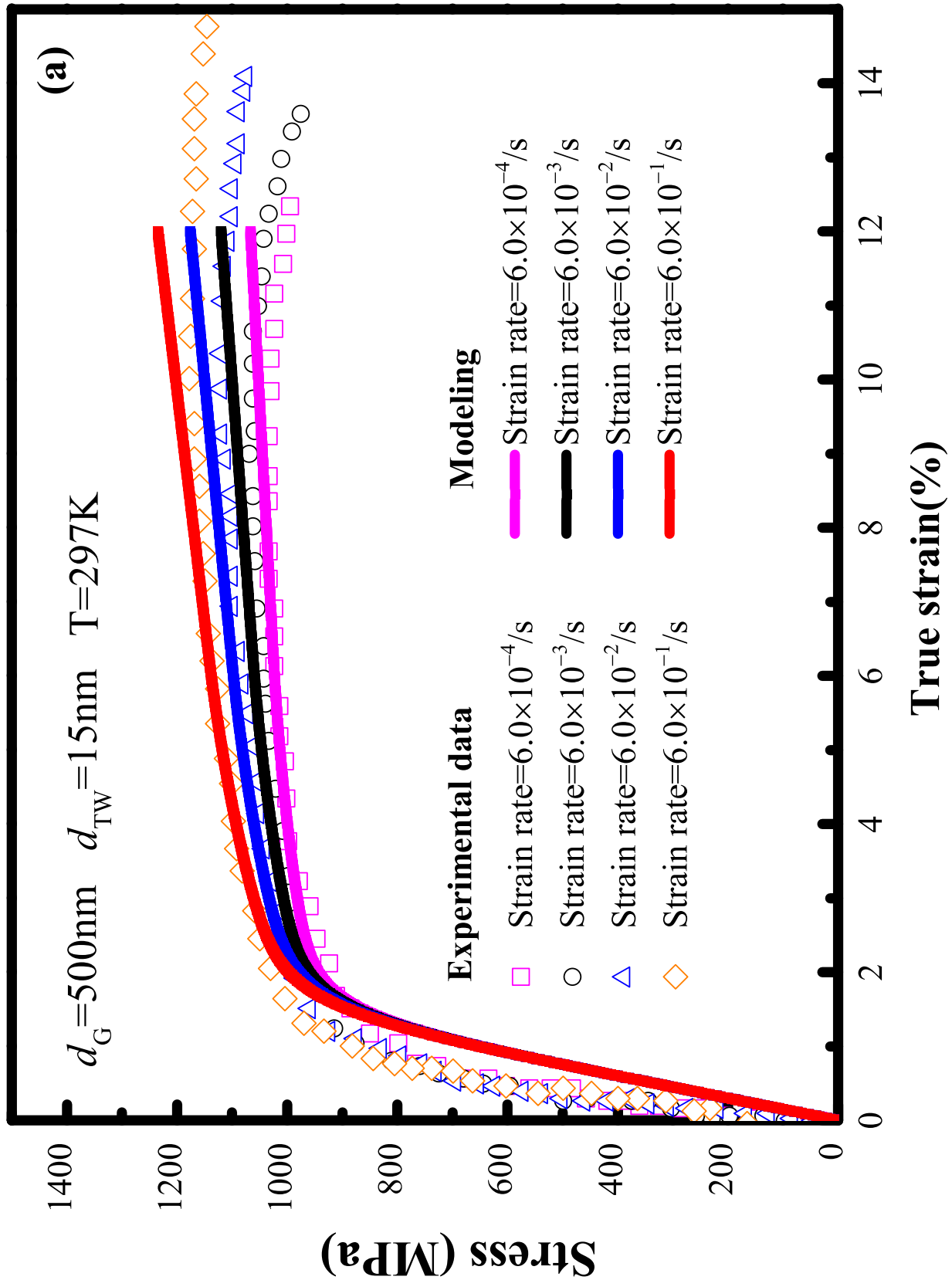
(a)
d_G=500nm d_{TW}=15nm T=297K
Experimental data
Strain rate=6.0×10^{-4}/s
Strain rate=6.0×10^{-3}/s
Strain rate=6.0×10^{-2}/s
Strain rate=6.0×10^{-1}/s
Modeling
Strain rate=6.0×10^{-4}/s
Strain rate=6.0×10^{-3}/s
Strain rate=6.0×10^{-2}/s
Strain rate=6.0×10^{-1}/s
Stress (MPa)
True strain(%)
0
200
400
600
800
1000
1200
1400
0
2
4
6
8
10
12
14

Figure1b

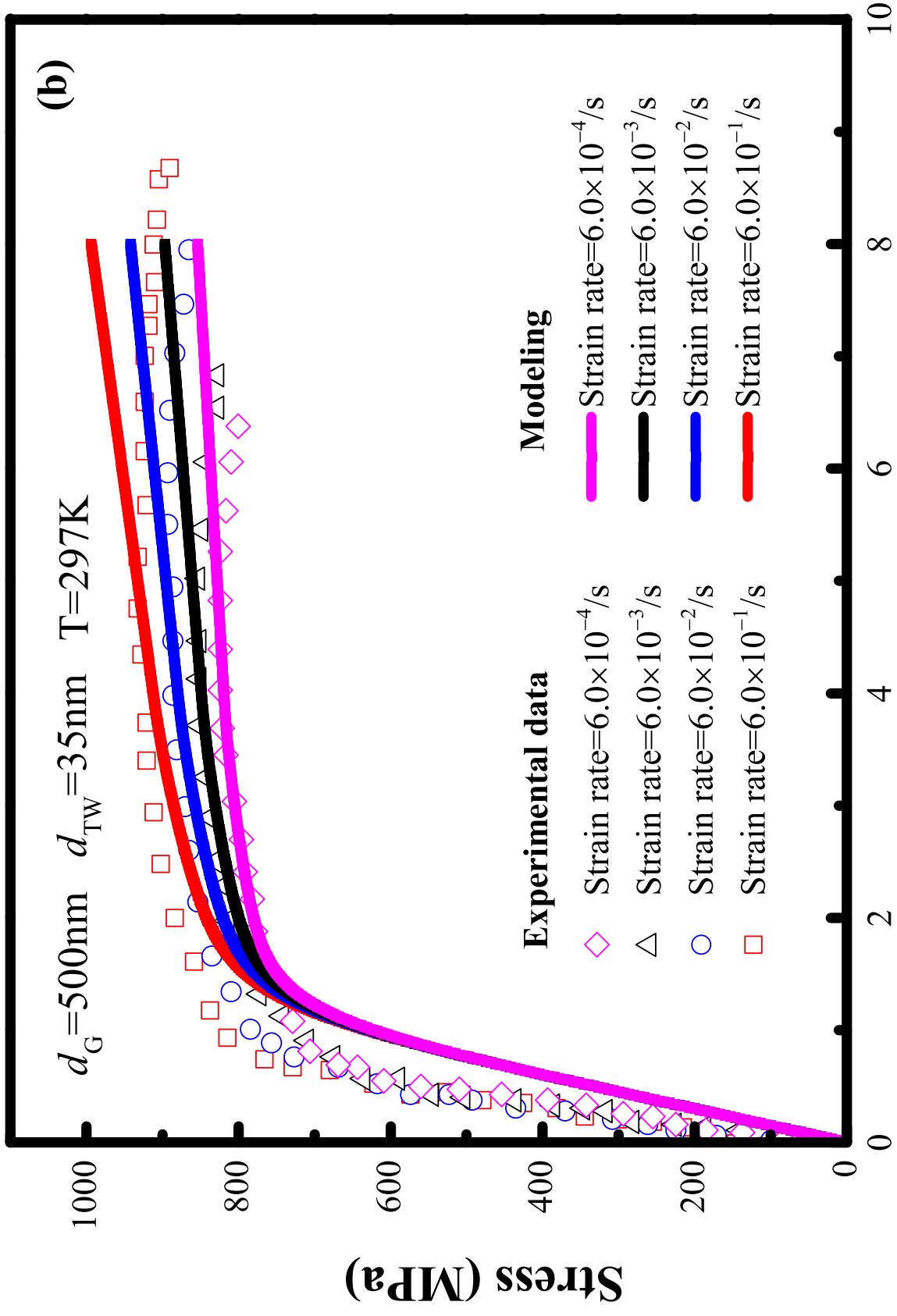
(b)
d_G=500nm d_{TW}=35nm T=297K
Experimental data
Strain rate=6.0×10^{-4}/s
Strain rate=6.0×10^{-3}/s
Strain rate=6.0×10^{-2}/s
Strain rate=6.0×10^{-1}/s
Modeling
Strain rate=6.0×10^{-4}/s
Strain rate=6.0×10^{-3}/s
Strain rate=6.0×10^{-2}/s
Strain rate=6.0×10^{-1}/s
Stress (MPa)
True strain(%)
0
200
400
600
800
1000
0
2
4
6
8
10

Figure1c

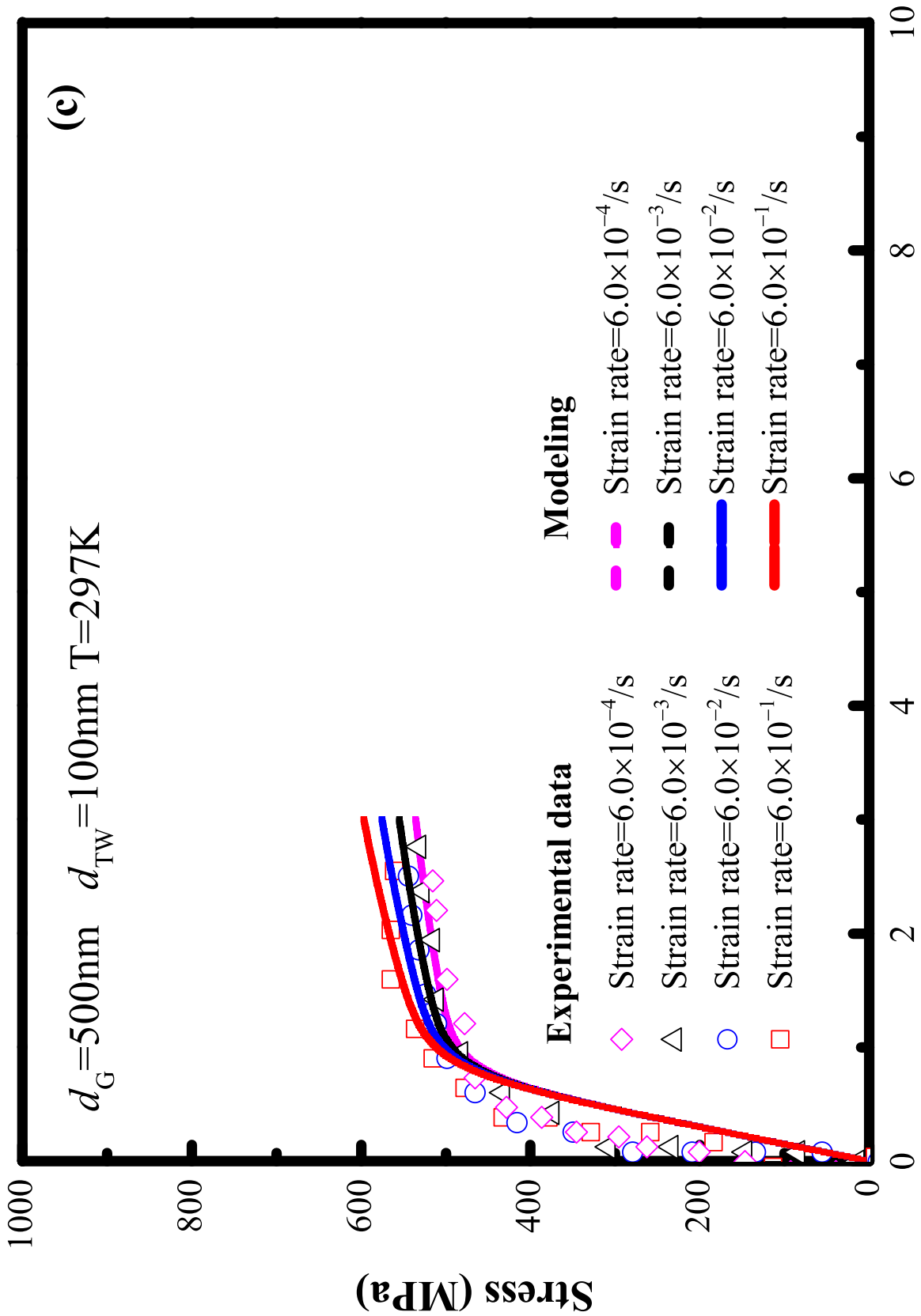
(c)
d_G=500nm d_{TW}=100nm T=297K
Experimental data
Strain rate=6.0×10^{-4}/s
Strain rate=6.0×10^{-3}/s
Strain rate=6.0×10^{-2}/s
Strain rate=6.0×10^{-1}/s
Modeling
Strain rate=6.0×10^{-4}/s
Strain rate=6.0×10^{-3}/s
Strain rate=6.0×10^{-2}/s
Strain rate=6.0×10^{-1}/s
Stress (MPa)
True strain(%)
0
200
400
600
800
1000
0
2
4
6
8
10

Figure2a

Click here to download high resolution image

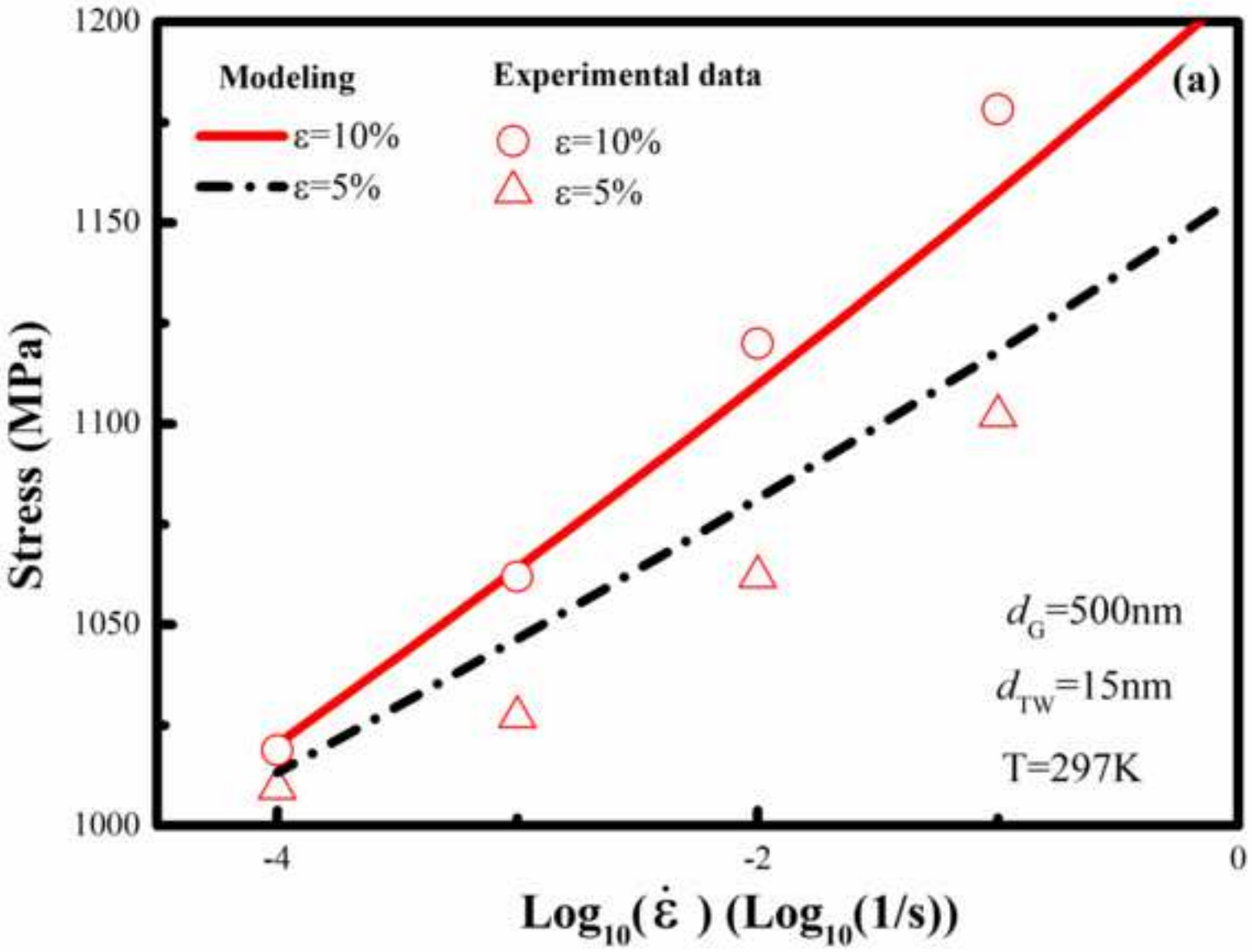

Figure2b

Click here to download high resolution image

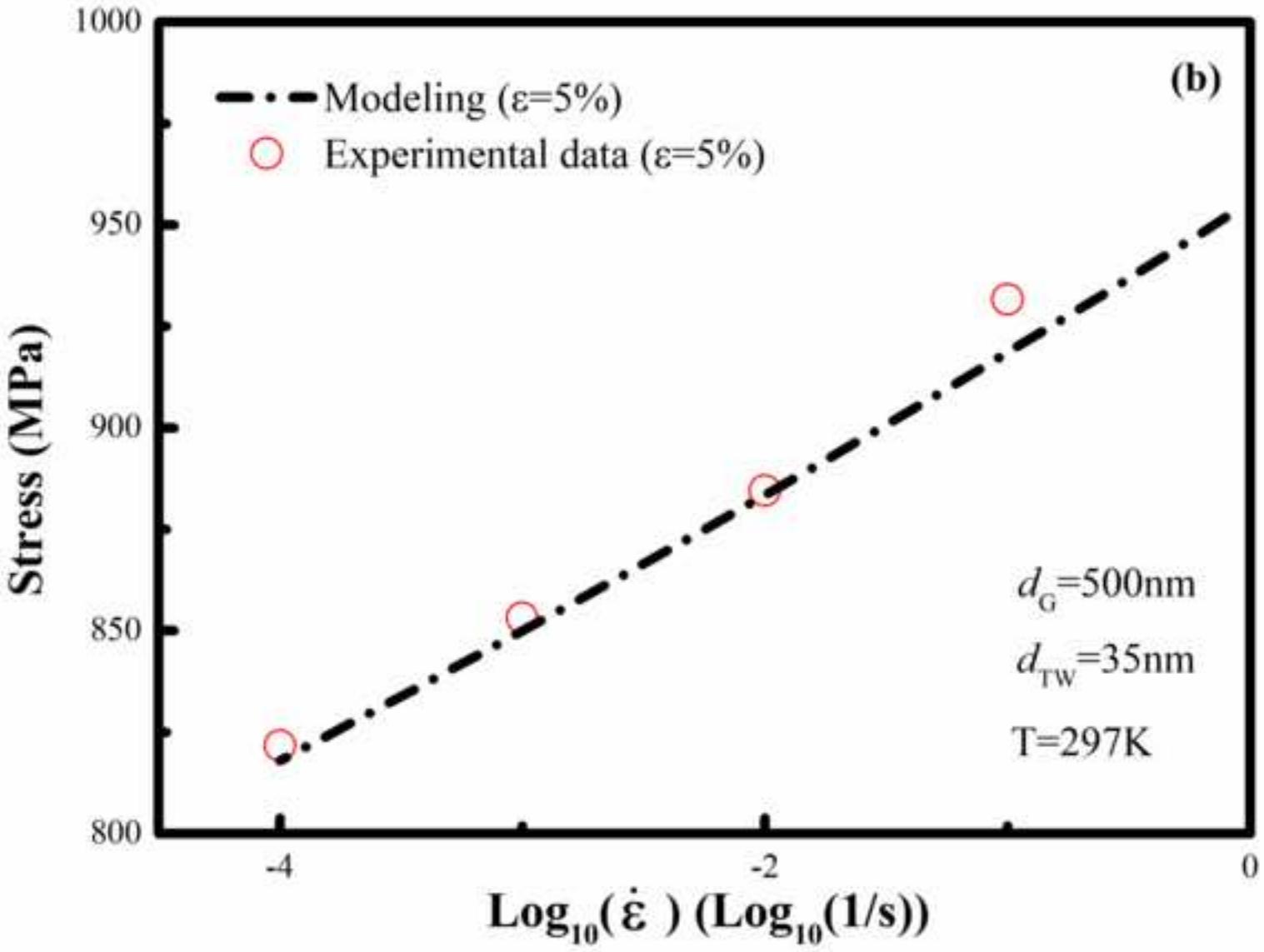

Figure2c

Click here to download high resolution image

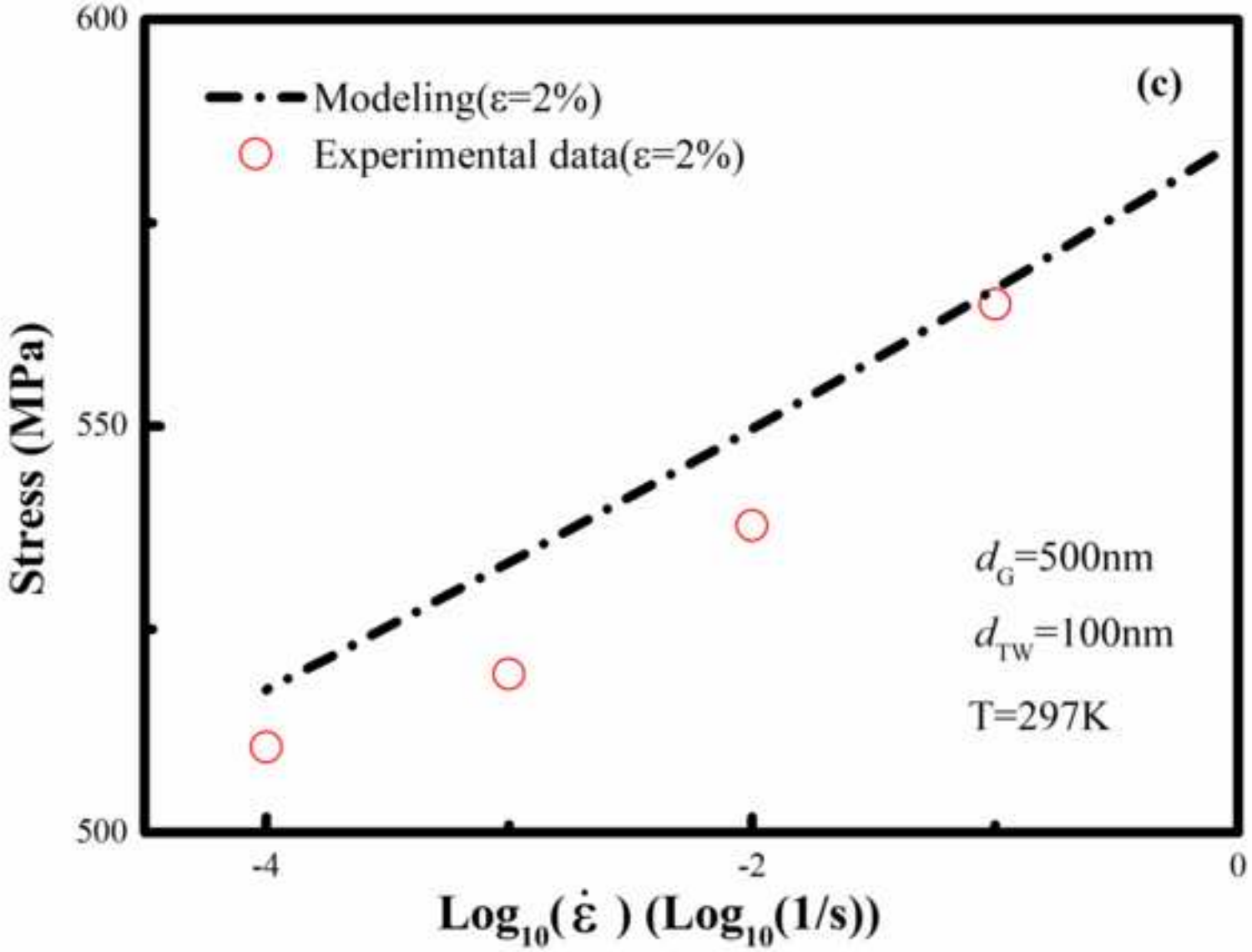

Figure2d

Click here to download high resolution image

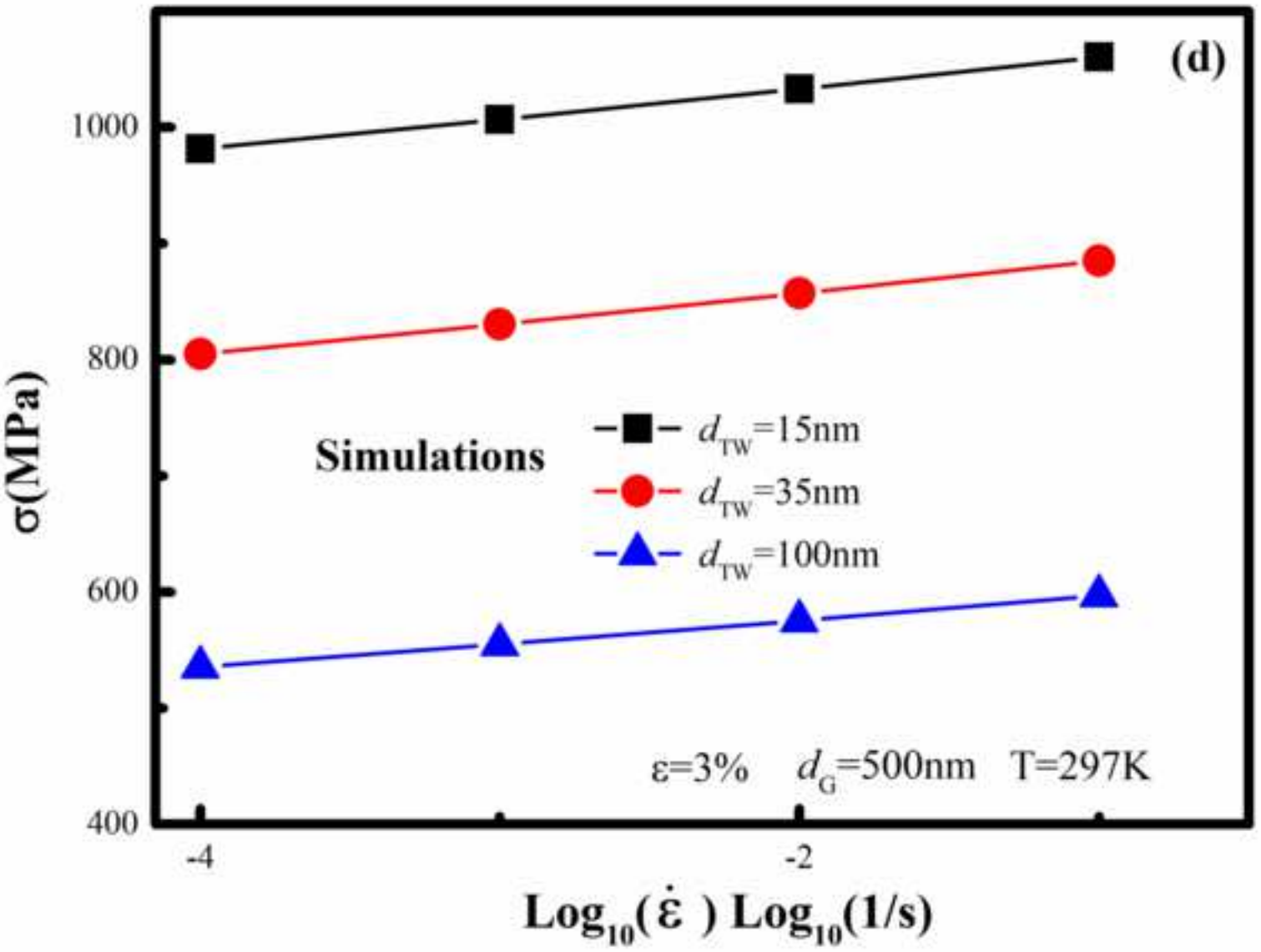

Figure3a

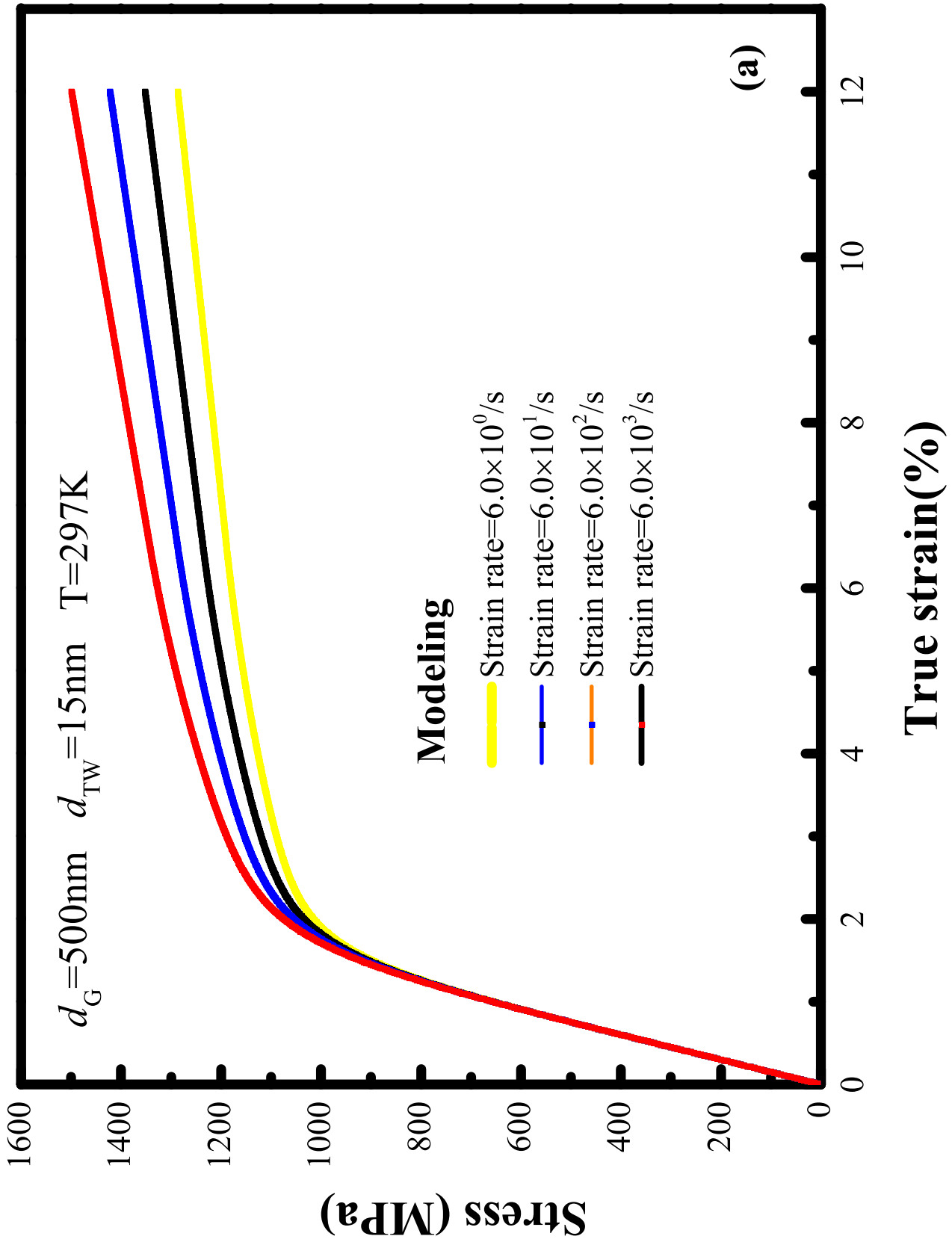
(a)
d_G=500nm d_{TW}=15nm T=297K
Modeling
Strain rate=6.0×10^0/s
Strain rate=6.0×10^1/s
Strain rate=6.0×10^2/s
Strain rate=6.0×10^3/s
Stress (MPa)
True strain(%)
0
200
400
600
800
1000
1200
1400
1600
0
2
4
6
8
10
12

Figure3b

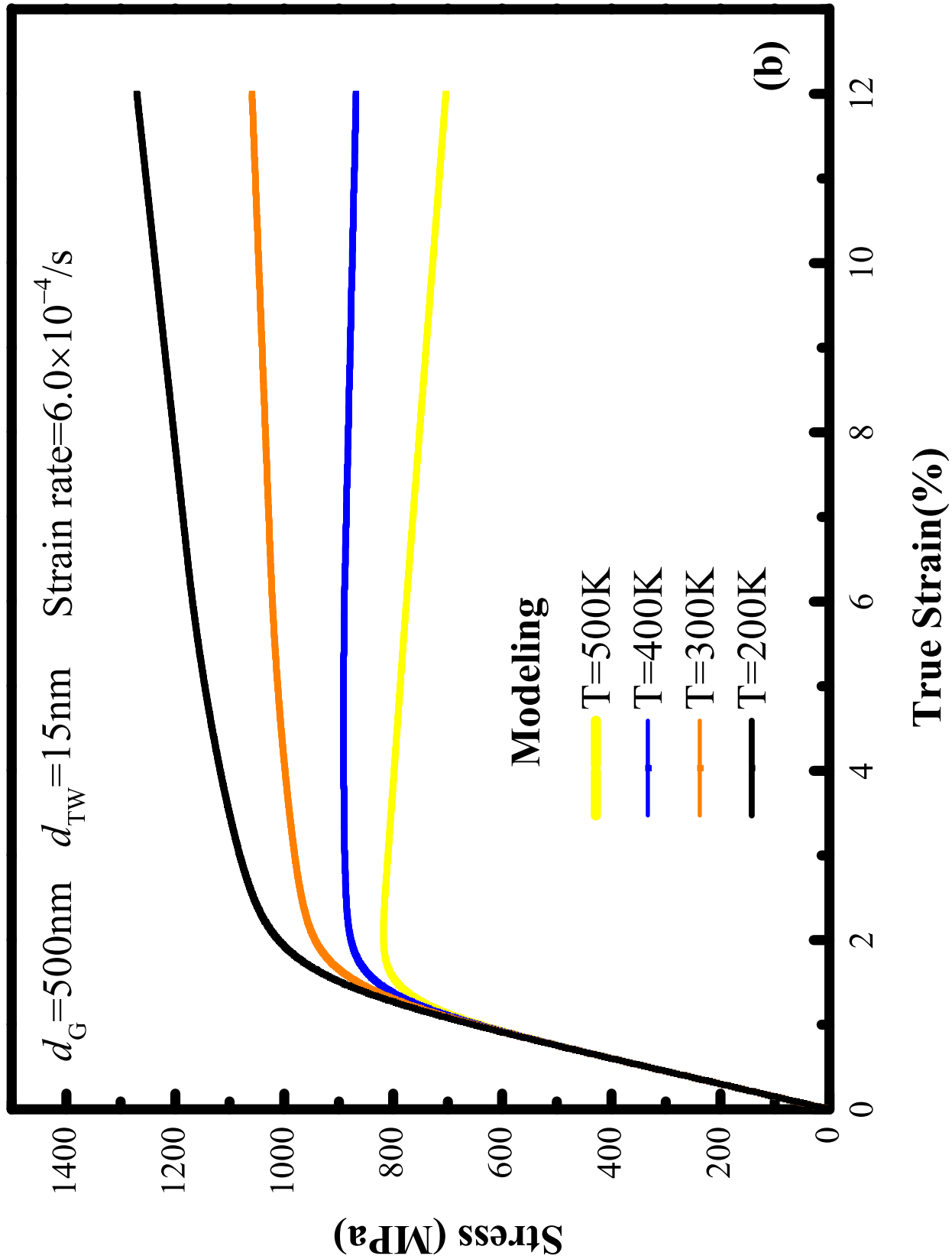
(b)
d_G=500nm d_{TW}=15nm Strain rate=6.0×10^{-4}/s
Modeling
T=500K
T=400K
T=300K
T=200K
Stress (MPa)
True Strain(%)
0
200
400
600
800
1000
1200
1400
0
2
4
6
8
10
12

***Declaration of Interest Statement**

Declaration of interests

☒ The authors declare that they have no known competing financial interests or personal relationships that could have appeared to influence the work reported in this paper.

☐The authors declare the following financial interests/personal relationships which may be considered as potential competing interests:

***Author Contributions Section**

CRediT author statement

Guo Zizheng, Wu Kai: Data curation, Original draft preparation. **Ruan Haihui, Zhu Linli***:* Supervision, Reviewing and Editing.